Journal of Engineering Mathematics **44:** 125–145, 2002.

Semi-analytical solutions for continuous-flow microwave reactors

M. Z. C. LEE and T. R. MARCHANT
School of Mathematics and Applied Statistics, The University of Wollongong, Wollongong, 2522, N.S.W., Australia.

Received 15 December 2001; accepted in revised form 28 May 2002

Abstract. A prototype chemical reaction is examined in both one and two-dimensional continuous-flow microwave reactors, which are unstirred so the effects of diffusion are important. The reaction rate obeys the Arrhenius law and the thermal absorptivity of the reactor contents is assumed to be both temperature- and concentration-dependent. The governing equations consist of coupled reaction-diffusion equations for the temperature and reactant concentration, plus a Helmholtz equation describing the electric-field amplitude in the reactor. The Galerkin method is used to develop a semi-analytical microwave reactor model, which consists of ordinary differential equations. A stability analysis is performed on the semi-analytical model. This allows the stability of the system to be determined for particular parameter choices and also allows any regions of parameter space in which Hopf bifurcations (and hence periodic solutions called limit-cycles) occur to be obtained. An excellent comparison is obtained between the semi-analytical and numerical solutions, both for the steady-state solution and for time-varying solutions, such as the limit-cycle.

Key words: Hopf bifurcations, limit-cycles, microwave-assisted chemistry, reaction-diffusion equations, stability analysis

1. Introduction

Microwave-assisted chemistry is an emerging area of experimental and theoretical study due to its advantages over conventional chemical reactors. Some of these advantages are increased yield, shorter processing times and cleaner operating conditions. The applications which are aided by using microwave heating include the synthesis of organic compounds and pharmaceuticals, soil decontamination, oil recovery, desorption of trace components and catalytic reactions, see [1] or [2] for details of these applications.

It is well known that controlled uniform heating is difficult to achieve with microwave radiation as thermal runaway (ignition) can occur in some materials for a small increase in incident power. The phenomenon of thermal runaway, due to the temperature dependence of the material properties, is analogous to the combustion of an exothermic chemical reactant or a flashover in a fire. Moreover, the temperature versus microwave power relationship is described by the classical S-shaped curve of combustion theory, hence thermal runaway occurs at a critical power level, when the temperature jumps from the low (cool) branch to the upper (hot) solution branch.

The equations governing the microwave heating of a material are Maxwell's equations, governing the propagation of microwave radiation through the material, and the forced heat equation, governing the heat absorption and the resultant heat diffusion. It is also necessary to calculate the electromagnetic field within the waveguide or microwave cavity, inside which the material is processed. In applications involving microwave-assisted chemistry additional

reaction-diffusion equations are needed, to describe the concentrations of chemical species associated with the reaction(s) occurring in the microwave reactor.

The prediction of temperature and concentration profiles requires the numerical solution of Maxwell's equations within the reactor and the waveguide or microwave cavity, coupled with the solution of a set of reaction-diffusion equations within the microwave reactor. For reactors with a realistic two- or three-dimensional geometry this approach is computationally expensive, and unlikely to be of much practical use, particularly if real-time feedback control over the reactor is required. Hence the development of semi-analytical models of microwave heating has generated a lot of interest in the last few years. Moreover, the governing partial differential equations are unsuited to the analysis techniques used in combustion theory.

The heating of a two-dimensional slab in a long rectangular waveguide propagating the TE_{10} waveguide mode was considered in [3]. The temperature dependency of the electrical conductivity and the thermal absorptivity were assumed to be governed by an Arrhenius-type law. Semi-analytical solutions were found for the steady-state temperature and the electric-field amplitude using the Galerkin method. The steady-state temperature-versus-power curve was found to be S-shaped. Examples were presented in the limits of small and large heat-loss and an excellent comparison with numerical solutions of the governing equations was obtained.

A simple control model for the microwave heating of ceramics in the small-Biot-number limit was developed in [4]. This control process mitigates against thermal runaway, and enables the desired steady-state to be easily reached. Averaging the forced heat equation gives an ordinary differential equation, which, when coupled with the control equation, describes the evolution of the temperature. The system exhibits qualitatively different behaviours, such as limit-cycles or oscillatory decay to the steady-state, depending on the parameter choices.

Feedback control of microwave-heated slabs in one and two-dimensional waveguides was considered in [5]. A semi-analytical feedback control model, consisting of ordinary differential equations, was developed. A local stability analysis allowed the feedback parameters for which Hopf bifurcations occur, to be predicted. An excellent comparison was obtained between numerical and semi-analytical solutions, for the transient evolution of the temperature, including examples describing limit-cycles.

The microwave heating of a solid combustible material was considered in [6], in order to model the combustion synthesis of ceramics and alloys. A one-step exothermic reaction with Arrhenius kinetics and a high activation energy was considered, with asymptotic solutions obtained using the Biot-number and the inverse activation energy as two small parameters. The ratio of these parameters was found to be important in determining the position of the ignition site in the material.

A one-dimensional model of microwave-enhanced chemical vapour infiltration was considered in [7]. In this process a silicon carbide composite is generated by the forcing of reactant gases into an Alumina preform. A set of coupled reaction-diffusion equations were obtained describing the temperature, gas concentration, electric-field amplitude and pore radius in the preform. Numerical solutions were obtained of a sharp-interface model and processing strategies discussed.

The design of a new continuous-flow well-stirred microwave reactor, and its testing on the organic synthesis of esters, was reported in [8]. The reaction takes place with the aid of a catalyst; the advantage of the microwave reactor is that the catalyst has a much higher dielectric loss than the solvent containing the reactants. This allows the catalyst to be selectively heated, thus speeding up the reaction-rate, without significantly heating the solvent. Experiments

showed that, for the same bulk temperature of the solvent, the microwave reactor resulted in an increased yield and a faster reaction, compared to the conventional continuous-flow reactor.

Typically, coupling between the concentration of the reactant and the temperature in a chemical reactor occurs because the reaction is exothermic and it has a temperature-dependent reaction-rate, governed by the Arrhenius law. The Sal'nikov thermokinetic oscillator is an example of such a system, in which Hopf bifurcations (limit-cycles) can occur, see [9]. This coupling occurs for both conventional and microwave reactors, except of course, that the volumetric heating characteristic of microwave processing allows faster heating of the reactants than conventional heating does.

In this paper a different coupling mechanism between concentration and temperature is considered which is specific to microwave reactors, and for which there is no analogue in conventional reactors. The dielectric-loss of the reactant shall be assumed to be vastly greater than that of the reaction products, hence the thermal absorptivity (the dielectric-loss) will be a function of reactant concentration. This is likely to be a common scenario as, even for members of the same chemical family, the dielectric-loss varies dramatically. For example, at a microwave frequency of 10GHz, the dielectric-loss of methanol is an order of magnitude larger than that of ethanol. A similar dramatic difference in dielectric-loss occurs for Mono and Dichlorobiphenyl, in [10, pp. 362–363].

Experimental evidence of this phenomenon is provided in [11], who showed that the dielectric-loss of an epoxy resin decreases significantly, by up to 30%, as the cross-linking curing reaction proceeds. Another experimental scenario in which this type of coupling would be important is microwave catalysis (see [8]), involving a lossy catalyst consumed in the reaction.

In Section 2 governing equations are developed for the reactant concentration, the temperature and the electric-field amplitude for both one and two-dimensional continuous-flow microwave reactors. Note that the reactors are not stirred so diffusion is important. In Section 3 a semi-analytical model, consisting of ordinary differential equations, is obtained for the reactors using the Galerkin method. In Section 4 the results are presented and discussed. The stability is determined using a local stability analysis of the semi-analytical model. This also allows regions of parameter space, in which limit-cycles occur, to be identified. Comparisons are made between the semi-analytical model and numerical solutions of the governing equations, both for the steady-state response curves and in the concentration versus temperature phase-plane. An example of a limit-cycle is also considered in detail. Appendix A contains integrals associated with the semi-analytical solution whilst Appendix B contains details of the numerical scheme used to solve the governing equations.

2. Governing equations

Problems involving microwave-assisted chemistry require the solution of Maxwell's equations, which govern the propagation of the microwave radiation, and coupled reaction-diffusion equations, which govern the absorption and diffusion of heat and the creation, decay and diffusion of the relevant chemical species. Maxwell's equations of electromagnetism are given by

$$\nabla \cdot \mathbf{D} = \nabla \cdot (\epsilon \mathbf{E}) = \rho, \quad \nabla \cdot \mathbf{B} = \nabla \cdot (\mu \mathbf{H}) = 0,$$
$$\nabla \times \mathbf{E} = -\frac{\partial}{\partial t}(\mu \mathbf{H}), \quad \nabla \times \mathbf{H} = \frac{\partial}{\partial t}(\epsilon \mathbf{E}) + \sigma \mathbf{E}, \tag{1}$$

based on the assumption that the material is homogeneous, isotropic and Ohmic, so that the current **J** and the displacement current **D** are both proportional to the electric field **E** and the magnetic field strength **H**. Here σ is the electrical conductivity, ϵ is the electrical permittivity and μ is the magnetic permeability. In general, all material properties are temperature-dependent. Also, as dielectric materials are being considered, there are no external charges ($\rho = 0$) or currents. Maxwell's equations are coupled with a reaction-diffusion equation for the temperature,

$$T_t = \nabla^2 T + \gamma(T, c)\mathbf{E} \cdot \overline{\mathbf{E}}, \tag{2}$$

where γ is the thermal absorptivity and c is the concentration of some chemical species. It is assumed that the thermal absorptivity is both temperature- and concentration-dependent. The thermal absorption depends on the square of the electric-field amplitude, based on the assumption that the heating occurs on a length scale much greater than a microwave-length, so that in (2) the absorption of heat is averaged over a wavelength. Alternatively, (2) can be obtained by assuming that the time taken for heat to diffuse a microwave-length is much greater than the period of the microwave radiation.

At the reactor boundaries convective heat-loss occurs,

$$\nabla T \cdot \mathbf{n} + B_i(T - T_a) = 0, \tag{3}$$

where B_i is the Biot-number, a measure of the relative effect of convective heat-loss compared to conduction, **n** is the normal to the boundary and T_a is the ambient temperature. In the small heat-loss limit ($B_i \to 0$) a zero heat-flux boundary condition results, while in the large heat-loss limit ($B_i \to \infty$) a fixed-temperature boundary condition is obtained. The boundary conditions for the electric-field at the interfaces with free space are

$$(\mathbf{E} - \mathbf{E}_f) \times \mathbf{n} = 0, \quad (\mathbf{H} - \mathbf{H}_f) \times \mathbf{n} = 0, \quad (\epsilon \mathbf{E} - \epsilon_f \mathbf{E}_f) \cdot \mathbf{n} = 0, \tag{4}$$

where $\mathbf{E}_f$ and $\mathbf{H}_f$ are the electric and magnetic fields in the free space incident upon the material; ϵ and ϵ_f are the electrical permittivities of the material and free space, respectively. Hence the tangential components of **E** are continuous across the dielectric interface, while the normal component of **E** is discontinuous. On the surface of the waveguide

$$\mathbf{E} \times \mathbf{n} = 0, \tag{5}$$

as there is no electric-field in a conductor.

A prototype chemical reaction

$$C \to P, \quad \text{rate } = r_1 c \mathrm{e}^{-\frac{E_a}{T}}, \tag{6}$$

is considered, which represents the one-step decay of a chemical reactant C to a product P. The reaction rate is proportional to the concentration of the reactant, c, and is temperature-dependent, with the rate governed by the Arrhenius law. The parameter r_1 is a rate constant, while E_a is the activation temperature. It is assumed that the heat of reaction is small, compared to the heat absorbed by the microwave energy, and hence can be ignored. Also,

the dielectric-loss of the reaction's products is assumed to be negligible, compared to the dielectric-loss of the reactant. This means that the thermal absorptivity is proportional to the concentration of the reactant, but not dependent on the concentration of the products. The governing equation and boundary condition for the reactant is

$$c_t = \nabla^2 c - r_1 c \mathrm{e}^{-\frac{E_a}{T}}, \quad \nabla c \cdot \mathbf{n} + N(c - c_a) = 0, \tag{7}$$

where c_a is the ambient reactant concentration and N is the Sherwood-number, the mass-diffusion equivalent of the Biot-number.

2.1. The two-dimensional microwave reactor

The microwave reactor has non-dimensional length and width of two, and completely fills the cross-section of the infinitely long rectangular waveguide. The reactor fits into a slot cut in the waveguide. Slotted waveguides represent a common experimental tool, allowing the input of materials to be processed, whilst avoiding significant radiation leakage. The radiation propagates in the positive x-direction and consists of the fundamental transverse-electric waveguide mode, TE_{10}, the usual choice for single-mode commercial waveguides. The walls of the reactor at $x = \pm 1$ are made of an impermeable material which is transparent to the microwave radiation. At $y = \pm 1$ the reactor boundaries are porous membranes. These allow diffusion into the reactor, from reservoirs containing the reactant at a constant concentration.

The electric and magnetic fields can then be written as

$$E = U(x, y)\mathrm{e}^{-\mathrm{i}\omega t}\mathbf{k}, \quad H = V_1(x, y)\mathrm{e}^{-\mathrm{i}\omega t}\mathbf{i} + V_2(x, y)\mathrm{e}^{-\mathrm{i}\omega t}\mathbf{j}, \tag{8}$$

where the time-harmonic form is used. Substituting (8) in Maxwell's equations (1) gives the governing equations as

$$\begin{aligned} &U_{xx} + U_{yy} + {k_1}^2(1 + \mathrm{i}\sigma)U = 0, \\ &T_t = T_{xx} + T_{yy} + \beta c f(T)|U|^2, \\ &c_t = c_{xx} + c_{yy} - \delta c \mathrm{e}^{-\frac{1}{T}}, \end{aligned} \tag{9}$$

where the temperature has been scaled with respect to the activation temperature, the reactant with respect to the reservoir concentration and the electric-field with respect to its incident amplitude. The parameters are k_1, the wavenumber of the radiation in the reactor, σ, the electrical conductivity and δ, a reaction rate-constant. The thermal absorptivity $\gamma = \beta c f(T)$, where $f(T)$ is the form of the temperature dependency and β is the microwave power. We choose the electrical conductivity to be proportional to the thermal absorptivity, $\sigma = \alpha c f(T)$, as physically it is expected from conservation of energy that the energy lost from the microwaves is absorbed as heat.

Note that the scaled electrical conductivity in (9) is equal to $\sigma/\omega\epsilon$, in terms of the unscaled variables. The electrical permittivity is often written as the complex expression $\epsilon = \epsilon' + \mathrm{i}\epsilon''$, where ϵ' is the dielectric constant and ϵ'' is the dielectric loss. The scaled electrical conductivity is then given by $\sigma = \epsilon''/\epsilon'$, and is referred to as the loss tangent.

The TE_{10} mode has the form

$$U = \cos(\frac{\pi y}{2m})\mathrm{e}^{\mathrm{i}k_r(x+1)},$$
$$V_1 = \frac{\mathrm{i}\pi}{2\mu\omega m}\sin(\frac{\pi y}{2m})\mathrm{e}^{\mathrm{i}k_r(x+1)}, \tag{10}$$
$$V_2 = -\frac{k_r}{\mu\omega}\cos(\frac{\pi y}{2m})\mathrm{e}^{\mathrm{i}k_r(x+1)},$$

where $k_r = \sqrt{k^2 - \frac{\pi^2}{4m^2}}$ and k is the wavenumber of the microwave radiation in free space. For the microwaves to propagate in the waveguide $k > \frac{\pi}{2m}$, the cut-off wavenumber. The boundary conditions are

$$U_x + \mathrm{i}k_r U = 2\mathrm{i}k_r \cos(\frac{\pi y}{2m}), \quad x = -1,$$
$$U_x - \mathrm{i}k_r U = 0, \quad x = 1,$$
$$U = 0, \quad y = \pm m, \tag{11}$$
$$T = T_a, \quad x = \pm 1, \quad y = \pm 1$$
$$c_x = 0, \quad x = \pm 1, \quad c = 1, \quad y = -1, \quad c = 0, \quad y = 1,$$

A fixed temperature boundary condition is assumed at all the reactor's surfaces. A fixed concentration boundary condition is applied at both reservoirs locations, $y = \pm 1$, while at $x = \pm 1$ a zero-mass-flux condition is imposed. To facilitate the transport of reactant into the microwave reactor, the reservoir at $y = -1$ contains reactant (at a scaled concentration of unity), while the reservoir at $y = 1$ contains no reactant. The initial conditions are

$$T = T_a, \quad c = \frac{1-y}{2}, \quad \text{at } t = 0. \tag{12}$$

2.2. The one-dimensional microwave reactor

In the one-dimensional case we assume that the width of the reactor is small and hence the y-variations in the electric-field amplitude, temperature and concentration are negligible. Hence the temperature and concentration profiles in the y-direction are nearly uniform and the second and third of (9) can be integrated in the y-direction. See [12] for a description of this averaging for a problem involving the microwave heating of ceramics in the small-Biot-number limit.

The governing equations become

$$U_{xx} + {k_1}^2(1 + \mathrm{i}\sigma)U = 0,$$
$$T_t = T_{xx} + \beta c f(T)|U|^2 + g(T_a - T), \tag{13}$$
$$c_t = c_{xx} - \delta c \mathrm{e}^{-\frac{1}{T}} + r(1-c),$$

where two new parameters, g and r, have been introduced. The parameter r represents the rate at which fresh reactant of concentration unity is exchanged with the reactor contents. The parameter g is the rate of heat-transfer between the reactor and the reactant reservoirs, which are at the ambient temperature. With no electric-field ($U = 0$) this system represents a continuous-flow unstirred reactor (CFUR), see, for example, [13]. Here the CFUR is subject to plane microwave radiation, incident at $x = -1$. The boundary conditions are

$$\begin{aligned} &U_x + \mathrm{i}kU = 2\mathrm{i}k, \quad x = -1, \quad U_x - \mathrm{i}kU = 0, \quad x = 1, \\ &T = T_a, \ \ c_x = 0, \ \ x = \pm 1, \end{aligned} \tag{14}$$

where fixed-temperature and zero-mass-flux boundary conditions apply at $x = \pm 1$. The initial conditions are

$$T = T_a, \ \ c = 0, \ \ \text{at } t = 0. \tag{15}$$

3. Semi-analytical solutions

In this section the semi-analytical model for the one- and two-dimensional microwave reactors is presented. The Galerkin method is used to obtain ordinary differential equations, which describe the evolution of the temperature, concentration and the electric-field amplitude in the microwave reactor.

3.1. The Arrhenius law and its approximation

The temperature-dependent rate of reaction in (9) is governed by the Arrhenius law, which in its scaled form is

$$\mathrm{Ar}(T) = \mathrm{e}^{-\frac{1}{T}}. \tag{16}$$

When the temperature is zero, so is the reaction-rate ($\mathrm{Ar}(0) = 0$) while as the temperature becomes large, $T \to \infty$, then the reaction rate is bounded, $\mathrm{Ar}(T) \to 1$. The Arrhenius law is not amenable for analytical work, so a rational-cubic function is chosen to approximate it. This function has the form

$$r_c(T) = \frac{R_1(T)}{R_2(T)} \quad \text{where} \quad R_i(T) = \sum_{j=0}^{3} r_{i,j} T^j, \quad i = 1, 2\,, \tag{17}$$

where the parameters

$$r_{10} = 0, \ r_{13} = r_{23} = 1, \tag{18}$$

are chosen for the rational-cubic function so it is the same as (16) in the limits of small and large temperatures. In order to obtain a good fit between the rational-cubic function and the Arrhenius law over the whole temperature range, the remaining parameters are chosen by the least squares method. The least squares method gives the rational-cubic parameters as

$$\begin{aligned} &r_{11} = 0{\cdot}01455, \ \ r_{12} = -0{\cdot}2451, \ \ r_{20} = 0{\cdot}07387, \\ &r_{21} = 0{\cdot}2617, \ \ r_{22} = 0{\cdot}7560. \end{aligned} \tag{19}$$

To graphical resolution there is no difference between the Arrhenius law (16) and the rational cubic (17) with the parameters (18) and (19), indicating that this approximation method is extremely accurate. See [3] for an example of the use of an Arrhenius-type law in the microwave heating of two-dimensional slabs.

The temperature dependence of the thermal absorptivity and electrical conductivity of the reactant, $f(T)$, can have exponential, Arrhenius or power-law form. See [14] for a discussion

of this dependency for some real dielectric materials. In this paper, for convenience, we let the temperature dependency $f(T)$, be equal to the Arrhenius law (16).

3.2. THE GALERKIN METHOD

The semi-analytical model for the two-dimensional microwave reactor is now derived. The model for the one-dimensional reactor, which follows a similar derivation, is then presented. Firstly, the governing equations (9) are written in the form

$$\begin{aligned} &R_2(T)T_t = T_{xx}R_2(T) + T_{yy}R_2(T) + \beta c R_1(T)|U|^2, \\ &R_2(T)c_t = c_{xx}R_2(T) + c_{yy}R_2(T) - \delta c R_1(T), \\ &U_{xx}R_2(T) + U_{yy}R_2(T) + k_1^2(R_2(T) + \mathrm{i}\alpha c R_1(T))U = 0, \end{aligned} \tag{20}$$

where the Arrhenius law (16) has been approximated by the rational-cubic function (17). Also, all equations have been multiplied by the denominator of the rational-cubic function so that analytically amenable expressions are obtained. A simple application of the Galerkin method is used, with the electric-field amplitude, temperature and the concentration each represented by one or two basis functions,

$$\begin{aligned} &T(x, y, t) = \phi_1, \quad c(x, y, t) = \phi_2, \quad U(x, y) = \phi_3, \\ &\phi_1 = T_a + T_0\phi_{11}, \phi_{11} = \cos(\frac{\pi}{2}x)\cos(\frac{\pi}{2}y), \\ &\phi_2 = \phi_{21} + C_0\phi_{22} + C_1\phi_{23}, \\ &\phi_{21} = \frac{1-y}{2}, \quad \phi_{22} = \cos(\frac{\pi}{2}y), \quad \phi_{23} = \cos(\pi x)\cos(\frac{\pi}{2}y), \\ &\phi_3 = \cos(\frac{\pi y}{2m})(A(a)\cosh(ax) + B(a)\sinh(ax)), \\ &A(a) = -\mathrm{i}k(a\sinh(a) - \mathrm{i}k\cosh(a))^{-1}, \\ &B(a) = \mathrm{i}k(a\cosh(a) - \mathrm{i}k\sinh(a))^{-1}, \end{aligned} \tag{21}$$

where T_0, C_0, C_1 and a are all parameters to be determined. The basis functions are chosen to satisfy the boundary conditions (11) exactly, but will satisfy averaged versions of the governing equations. The basis function for the electric-field amplitude is the exact solution in the case of constant electrical conductivity. Note the y-variation of the electric-field amplitude matches that of the TE_{10} mode. The basis functions for the temperature and concentration are motivated by the series solution for the diffusion equation and the nature of the physically realised solution. The linear term in ϕ_2 is due to the different concentrations in the two reactant reservoirs, located at $y = \pm 1$.

The averaged governing equations are

$$\begin{aligned} &< \omega_1\phi_{1t}R_2 > = < \omega_1((\phi_{1xx} + \phi_{1yy})R_2 + \beta|\phi_3|^2\phi_2 R_1) >, \\ &< \omega_{2n}\phi_{2t}R_2 > = < \omega_{2n}((\phi_{2xx} + \phi_{2yy})R_2 - \delta\phi_2 R_1) >, \\ &< \omega_3((\phi_{3xx} + \phi_{3yy})R_2 + k_1^2(R_2 + \mathrm{i}\alpha\phi_2 R_1)\phi_3) > = 0. \end{aligned} \tag{22}$$

Note that the angle brackets imply the integral of the enclosed quantity over the dimensions of the reactor, for example

$$< q >= \int_{-1}^{1}\int_{-1}^{1} q\,\mathrm{d}x\mathrm{d}y. \tag{23}$$

The integrals are weighted by ω_i, which are normally chosen as the basis functions themselves. We let $\omega_1 = \phi_{11}$, $\omega_2 = 1$, $\omega_2 = \phi_{22}$ and $\omega_3 = \phi_3^{-1}$. The weight for ω_3 is unusual; it is chosen as it gives a simple explicit expression for the decay rate,

$$a = (\frac{\pi^2}{4} - k_1^2(1 + \mathrm{i}\alpha I_{f1}{I_{f2}}^{-1}))^{\frac{1}{2}}. \tag{24}$$

The ordinary differential equations describing the evolution of the temperature and concentration are

$$\begin{aligned} T_0^{'} =& -\frac{\pi^2}{2}T_0 + \beta I_a I_b^{-1}, \\ C_0^{'}I_{ci2} + C_1^{'}I_{di2} =& -\frac{\pi^2}{4}C_0 I_{ci2} - \frac{5\pi^2}{4}C_1 I_{di2} \\ & -I_{ei} - C_0 I_{ci1} - C_1 I_{di1}, \quad i = 1, 2. \\ T_0(0) =& \; C_0(0) = C_1(0) = 0. \end{aligned} \tag{25}$$

where the integrals in (24) and (25) are defined as

$$\begin{aligned} &I_a =< \phi_{11}\phi_2 R_1|\phi_3|^2 >, \quad I_b =< \phi_{11}^2 R_2 >, \quad I_{cij} =< R_j\phi_{22}\phi_{23}^{i-1} >, \\ &I_{dij} =< R_j\phi_{23}^{i} >, \quad I_{ei} =< R_1\phi_{21}\phi_{23}^{i-1} >, \\ &I_{f1} =< \phi_2 R_1 >, \quad I_{f2} =< R_2 > . \end{aligned} \tag{26}$$

All these integrals are calculated using the symbolic manipulation package Maple, and appear in Appendix A. To simplify the calculation of I_a the square of the electric-field amplitude is written as

$$\begin{aligned} &|\phi_3|^2 = \cos^2(\frac{\pi y}{2m})(a_1\cosh(2ux) + b_1\cos(2vx)), \quad \text{where} \\ &a = u + \mathrm{i}v, \quad 2a_1 = A\overline{A} + B\overline{B}, \quad 2b_1 = A\overline{A} - B\overline{B}. \end{aligned} \tag{27}$$

The new parameters a_1, b_1, u and v are all real. Also note that the expression (27) contains only the symmetric terms of $|\phi_3|^2$ as the nonsymmetric terms integrate to zero in I_a.

The steady-state solution of (25) is

$$\begin{aligned} \beta =& \quad \frac{\pi^2}{2}T_0 I_b I_a^{-1}, \\ C_0 =& \; -4(5I_{e2}\pi^2 I_{d12} - 5\pi^2 I_{d22}I_{e1} + 4I_{e2}I_{d11} - 4I_{d21}I_{e1})D_3^{-1}, \\ C_1 =& \; -4(4I_{e1}I_{c21} + I_{e1}\pi^2 I_{c22} - 4I_{c11}I_{e2} - \pi^2 I_{c12}I_{e2})D_3^{-1}, \\ D_3 =& \; -20I_{c11}\pi^2 I_{d22} - 16I_{c11}I_{d21} - 5\pi^4 I_{c12}I_{d22} - 4\pi^2 I_{c12}I_{d21} \\ & +20\pi^2 I_{d12}I_{c21} + 5\pi^4 I_{d12}I_{c22} + 16I_{d11}I_{c21} + 4I_{d11}\pi^2 I_{c22}, \end{aligned} \tag{28}$$

which represent explicit expressions for the temperature versus power curve ($T_a + T_0$ versus β) and the concentration versus power curve ($\frac{1}{2} + C_0 + C_1$ versus β). Note that the temperature and concentration in the centre of the reactor are considered. By choosing a value of T_0 the

steady-state values of C_0 and C_1 can be found, by using the expressions in Appendix A. Then substitution of the temperature and concentration parameters in (24), gives the decay rate a, which in turn allows the power β to be calculated.

For the one-dimensional microwave reactor a similar procedure is followed to obtain the semi-analytical model, which is sketched below. The basis functions are

$$\begin{aligned} &T(x,t) = \phi_1, \;\; c(x,t) = \phi_2, \;\; U(x) = \phi_3, \\ &\phi_1 = T_a + T_0\phi_{11}, \;\; \phi_{11} = \cos(\tfrac{\pi}{2}x), \phi_2 = C_0 + C_1\phi_{21}, \\ &\phi_{21} = \cos(\pi x), \phi_3 = A(a)\cosh(ax) + B(a)\sinh(ax), \end{aligned} \tag{29}$$

where A and B are given in (21). The semi-analytical model of ordinary differential equations becomes

$$\begin{aligned} &T_0^{'} = -(\frac{\pi^2}{4} + g)T_0 + \beta I_a I_b^{-1}, \\ &C_0^{'} I_{ci2} + C_1^{'} I_{c,i+1,2} = r I_{ci2} - C_0(I_{ci2} + I_{ci1}) \\ &-C_1((\frac{\pi^2}{4} + r)I_{c,i+1,2} + I_{c,i+1,1}), \;\; i = 1, 2, \\ &a = \; \mathrm{i}(k_1^2 + \; \mathrm{i}\alpha(C_0 I_{c11} + C_1 I_{c21})I_{c12}^{-1})^{\frac{1}{2}}, \\ &T_0(0) = C_0(0) = C_1(0) = 0, \end{aligned} \tag{30}$$

which describes the evolution of the temperature and concentration and the decay of the electric-field amplitude. The integrals in (30) are defined as,

$$\begin{aligned} &I_a = < \phi_{11}\phi_2 R_1 |\phi_3|^2 >, \;\; I_b = < \phi_{11}^2 R_2 >, \\ &I_{cij} = < \phi_{21}^{i-1} R_j >, \;\; i = 1, 2, 3. \end{aligned} \tag{31}$$

The steady-state solution of (30) can be written as

$$\begin{aligned} &\beta = (\frac{\pi^2}{4} + g)T_0 I_b I_a^{-1}, \\ &C_0 = r((\frac{\pi^2}{4} + r)(I_{c32}I_{c12} - I_{c22}^2) + (I_{c31}I_{c12} - I_{c22}I_{c21}))D_1^{-1}, \\ &C_1 = r(I_{c22}I_{c11} - I_{c21}I_{c12})D_1^{-1}, \\ &D_1 = ((\frac{\pi^2}{4} + r)I_{c32} + I_{c31})(I_{c12} + I_{c11}) \\ &-((\frac{\pi^2}{4} + r)I_{c22} + I_{c21})(I_{c22} + I_{c21}), \end{aligned} \tag{32}$$

which again are explicit expressions for the steady-state temperature and concentration-versus-power curves.

4. Results and discussion

The steady-state and dynamical behaviour of the one and two-dimensional microwave reactors will be considered. Comparisons will be made between the semi-analytical and numerical

steady-state temperature and concentration-versus-power response curves. Also, a local stability analysis is performed on the semi-analytical models. This allows the stability of the steady-state solutions to be calculated and also gives the region of parameter space in which Hopf bifurcations, and the subsequent limit-cycles, occur. Comparisons are also made for the transient evolution of the temperature and concentration in a number of examples, including those for which limit-cycles occur.

4.1. Local stability analysis

The local stability can be found by perturbing the semi-analytical models about the steady-state solution,

$$T_0 = T_{0s} + \hat{T}_0, \quad C_0 = C_{0s} + \hat{C}_0, \quad C_1 = C_{1s} + \hat{C}_1, \tag{33}$$

where $|\hat{T}_0| \ll |T_{0s}|$, $|\hat{C}_0| \ll |C_{0s}|$ and $|\hat{C}_1| \ll |C_{1s}|$. Substituting (33) in the semi-analytical models gives the linear system $\mathbf{v}' = J\mathbf{v}$, where $\mathbf{v} = (\hat{T}_0, \hat{C}_0, \hat{C}_1)^T$ and J is the Jacobian matrix. For our models the eigenvalues, λ_e, of the Jacobian are described by the cubic equation

$$\lambda_e^3 + \alpha_1\lambda_e^2 + \alpha_2\lambda_e + \alpha_3 = 0, \tag{34}$$

where the coefficients, α_i, of the cubic equation are not presented here, but are calculated using the symbolic manipulation package, Maple. The stability of a particular steady-state solution is then found by solving (34), together with the steady-state equations, (28) or (32), using a standard root-finding routine from the IMSL library.

When the eigenvalues are negative and real or are complex with a negative real part, the steady-state solution is stable. Hopf bifurcations occur for this system when one pair of eigenvalues are purely imaginary, which implies $q = \alpha_3 - \alpha_1\alpha_2 = 0$. The region of parameter space in which Hopf bifurcations occur is found from the loci of the degenerate Hopf points, see [15]. There are two types of points to consider, the double-zero eigenvalue (DZE) and transversality (H2) degenerate Hopf points. The DZE condition implies that a pair of eigenvalues are zero while the H2 degeneracy occurs when two Hopf points on a solution branch merge with their eigenvalues having a non-zero imaginary part. The degenerate points are given by the conditions

$$\text{DZE}: \ \alpha_2 = \alpha_3 = 0, \ \ \text{H2}: \ \ q = \frac{\mathrm{d}q}{\mathrm{d}\beta} = 0, \tag{35}$$

together with the conditions for a steady-state solution.

For the H2 degeneracy condition the total derivative of q w.r.t. to β is taken, where the variables T_0, C_0 and C_1 and a all depend implicitly on β. This introduces new variables (such as $\mathrm{d}T_0/\mathrm{d}\beta$) so the system of equations is supplemented by the total derivative w.r.t. β of the steady-state equations. The relevant transcendental equations are found using Maple, and solved using a root-finding routine from the IMSL library. See [16] for further details on the application of this method for calculating degenerate Hopf points for a set of reaction-diffusion equations describing a cubic-autocatalytic reaction.

4.2. The one-dimensional microwave reactor

For the one-dimensional reactor, the common parameters are $k = k_1 = 1$, $g = 1$, $r = 0{\cdot}1$, $\alpha = 0{\cdot}1$, $\delta = 1$, $\Delta x = 0{\cdot}05$ and $\Delta t = 1 \times 10^{-4}$, unless otherwise stated. For all the

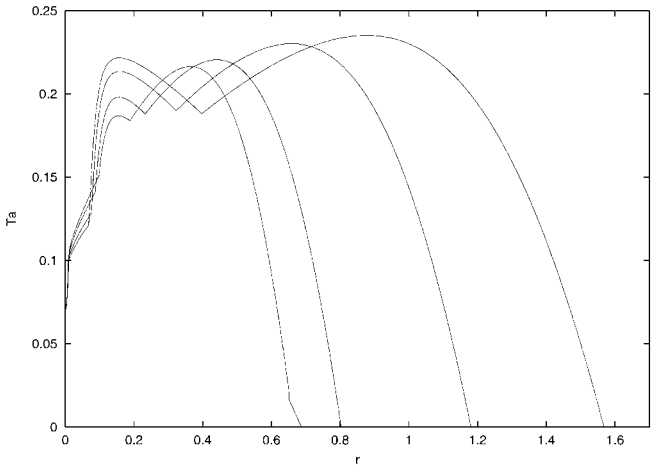

Figure 1. The region of (r, T_a) parameter space in which Hopf bifurcations are possible, for the one-dimensional reactor. Shown is the semi-analytical solution for $g = 0{\cdot}1$, 1, 4 and 8 (the curves from left to right).

steady-state S-shaped curves and phase-plane diagrams the temperature and concentration at the centre of the reactor, $x = 0$, is plotted.

Figure 1 shows the portion of (r, T_a) parameter space, in which Hopf bifurcations occur, for various values of g. These are $g = 0{\cdot}1$, 1, 4 and 8 (the curves from left to right). These curves are constructed from the union of the parameter regions bounded by the DZE and H2 Hopf degeneracy curves (35). For a given value of g Hopf bifurcations are possible for parameter values inside these curves. Hence, for a given value of g, there is a maximum value of ambient temperature T_a, for which Hopf bifurcations are possible. As g is increased the region of parameter space in which Hopf bifurcations occur also increases.

Figure 2(a) shows the steady-state temperature versus power ($T = T_a + T_0$ versus β) curve. Shown is the semi-analytical (solid line) and numerical solutions (dashed line). The ambient temperature $T_a = 0{\cdot}17$. The response curve is S-shaped hence ignition (or thermal runaway) occurs as the temperature jumps from the cool to the hot solution branch. The numerical solution is shown on the lower branch and a portion of the upper branch, where it is stable. An excellent comparison between the semi-analytical and numerical solution is obtained, with a difference of 3% at $\beta = 30$.

Qualitatively similar S-shaped response curves are obtained for the microwave heating of slabs, see, for example, [3]. For the heating of a slab, a simple stability analysis indicates that steady-state solutions on the lower and upper solution branches are stable nodes while steady-state solutions on the middle solution branch are unstable nodes. No oscillatory behaviour is possible as the semi-analytical model is described by only one ordinary differential equation. Here, the stability of the S-shaped response curve is much more complicated. The lower branch is stable, the majority of it being a stable node, except close to the bifurcation point, where it becomes a stable focus. Solutions on the middle branch are saddle points (unstable) while the lower portion of the upper branch, up to $\beta = 20{\cdot}9$, is an unstable focus. There is a point of Hopf bifurcation at $\beta = 20{\cdot}9$, beyond which the upper branch is a stable focus. Any initial condition in the parameter region where three steady-state solutions exists evolves to the lower (cool) steady-state solution, due to the instability of the upper branch. However, between the bifurcation point on the lower solution branch ($\beta = 16{\cdot}7$) and the point of Hopf bifurcation ($\beta = 20{\cdot}9$), no stable steady-state solution exists and a periodic solution (a

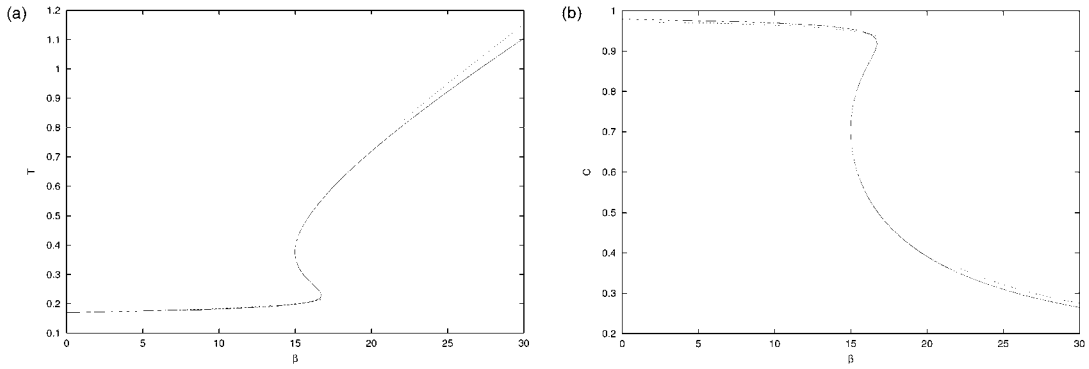

Figure 2. (a) is the steady-state temperature versus power curve ($T = T_a + T_0$ versus β) and (b) is the steady-state concentration versus power curve ($c = C_0 + C_1$ versus β) for the one-dimensional reactor. Shown is the semi-analytical (solid line) and numerical (dashed line) solutions. The ambient temperature $T_a = 0{\cdot}17$.

limit-cycle) occurs. Hence, in contrast to a microwave heated slab, oscillatory behaviour can occur for the reactor, with oscillatory convergence to the steady-state and periodic solutions both possible. In fact a jump from the low branch to the high branch will result in a stable limit-cycle occurring.

Figure 2(b) shows the steady-state concentration versus power ($c = C_0 + C_1$ versus β) curve. The ignition point represents a jump from the low conversion to the high conversion branch, as more reactant is consumed due to the higher temperature. Again the comparison with numerical solutions is excellent with only a small difference between the curves.

Figure 3 shows the steady-state (a) temperature, (b) concentration and (c) electric-field amplitude profiles. The ambient temperature $T_a = 0{\cdot}17$ and the power $\beta = 25$, hence this example is on the stable part of the upper branch of Figure 2. An excellent comparison is achieved for each of the profiles, indicating the accuracy of the semi-analytical solutions. The nearly uniform volumetric heating and convective heat-loss results in a central temperature peak forming in the reactor. This, in turn, speeds up the reaction in the centre of the reactor, which results in a central concentration trough. The electric field amplitude shows a small decay, of about 1%, through the microwave reactor.

Figure 4(a) and (b) shows the evolution of the solution in the concentration versus temperature phase-plane. For $g = 1$ the point $(r, T_a) = (0{\cdot}1, 0{\cdot}17)$ lies within the Hopf region given in Figure 1, so limit-cycles are possible. The parameters for Figure 4(a) are the same as for Figure 3, hence a steady-state solution results. The dominant eigenvalues, from the local stability analysis, are $\lambda_e = -0{\cdot}26 \pm \mathrm{i}1{\cdot}36$, which implies a stable focus. The oscillatory nature of the convergence to the steady-state can be clearly seen on the figure with a considerable overshoot in temperature before the steady-state is reached. For Figure 4(b) the power $\beta = 20$ while the other parameters are the same as for Figure 4(a). Now the steady-state solution is located lower down on the upper branch, in the unstable region. The dominant eigenvalues are $\lambda_e = 0{\cdot}07 \pm \mathrm{i}1{\cdot}06$, hence, as there is no other stable steady-state, a limit-cycle occurs. For both figures the comparison between the semi-analytical and numerical solutions is excellent. The semi-analytical amplitude of the limit-cycle is 2·29 (temperature) and 0·53 (concentration), while the period is 25·8. The numerical values are 2·43 and 0·52 for the temperature and concentration amplitudes, respectively, while the period is 24·2. Hence, the semi-analytical solution provides a very accurate estimate (no more than 5% error) of the limit-cycle's characteristics.

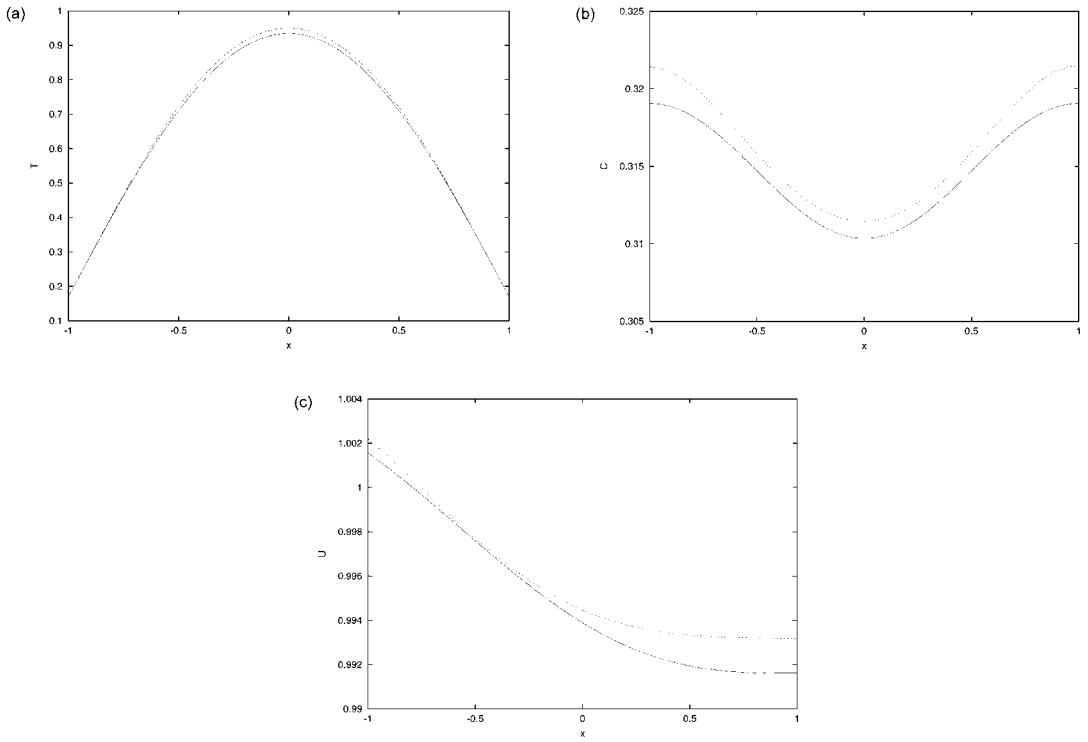

Figure 3. The steady-state (a) temperature, (b) concentration and (c) electric field amplitude profiles in the one-dimensional reactor. Shown is the semi-analytical (solid line) and numerical (dashed line) solutions. The parameters are $T_a = 0{\cdot}17$ and $\beta = 25$.

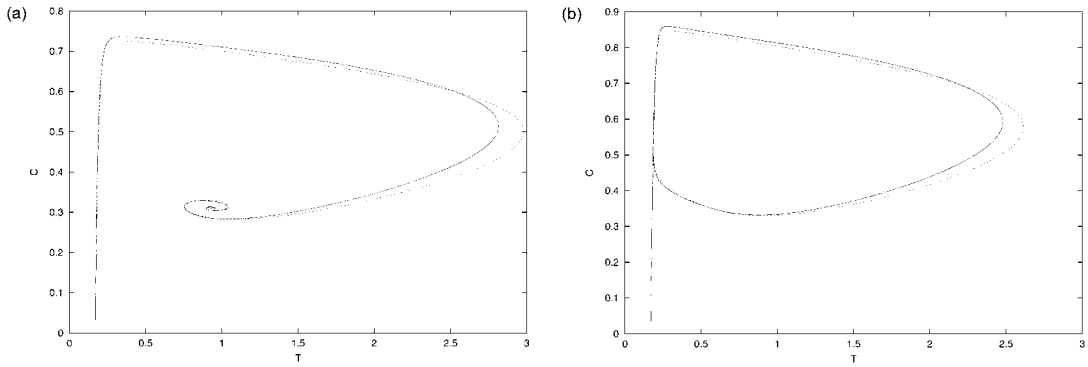

Figure 4. The evolution in the concentration versus temperature phase-plane, for the one-dimensional reactor. Shown is the semi-analytical (solid line) and numerical (dashed line) solutions. The ambient temperature $T_a = 0{\cdot}17$. The power for (a) is $\beta = 25$ and for (b) is $\beta = 20$.

4.3. THE TWO-DIMENSIONAL MICROWAVE REACTOR

For the two-dimensional microwave reactor the common parameters are $k = k_1 = 2$, $k_r = 1{\cdot}239$, $\delta = 1$, $\alpha = 0{\cdot}1$, $\Delta x = \Delta y = 0{\cdot}1$ and $\Delta t = 1 \times 10^{-4}$, unless otherwise stated. For all the steady-state S-shaped curves and phase-plane diagrams the temperature and concentration at the centre of the reactor, $(x, y) = (0, 0)$, are plotted.

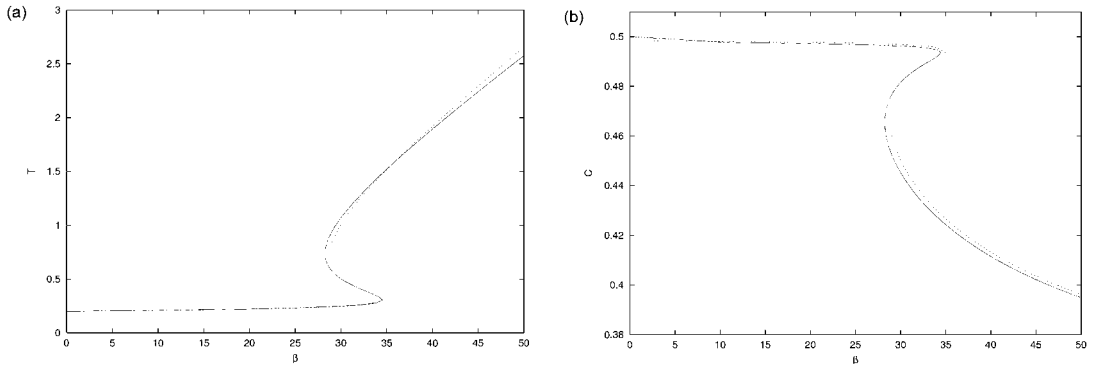

Figure 5. (a) is the steady-state temperature versus power curve ($T = T_a + T_0$ versus β) and (b) is the steady-state concentration versus power curve ($c = \frac{1}{2} + C_0 + C_1$ versus β) for the two-dimensional reactor. Shown is the semi-analytical (solid line) and numerical (dashed line) solutions. The ambient temperature $T_a = 0{\cdot}2$.

For the two-dimensional reactor no DZE or H2 Hopf degenerate points could be found, indicating that Hopf bifurcation points do not occur. So, unlike the one-dimensional reactor, cases of stable limit-cycles could not be identified.

Figure 5(a) shows the steady-state temperature-versus-power ($T = T_a + T_0$ versus β) curve, while 5(b) shows the steady-state concentration versus power ($c = \frac{1}{2} + C_0 + C_1$ versus β) curve. The ambient temperature $T_a = 0{\cdot}2$. Again the response curve is S-shaped, hence ignition (or thermal runaway) occurs as the temperature jumps from the cool to the hot solution branch and the concentration jumps from the low-conversion to the high-conversion branch. The numerical solution is shown on the lower and upper branches, where it is stable. An excellent comparison between the semi-analytical and numerical solution occurs for both figures. For example, the error in the semi-analytical temperature at $\beta = 50$ is only 3%.

The stability of the S-shaped response curves is as follows: the lower branch is a stable node, the middle branch a saddle point and the upper branch is also stable. The lower portion of the upper branch is a stable node, while between $\beta = 29{\cdot}3$ and $\beta = 59{\cdot}6$ it is a stable focus. Beyond $\beta = 59{\cdot}6$ it returns to a stable node. Hence limit-cycles are not possible for this example, but oscillatory convergence to upper branch steady-state solutions can occur.

Figure 6 shows contours of the steady-state temperature, (a) and (b), concentration, (c) and (d), and electric-field amplitude, (e) and (f), in the reactor. Shown is the semi-analytical (a, c, e) and numerical (b, d, f) solutions. The ambient temperature $T_a = 0{\cdot}2$ and the power $\beta = 40$, hence this example is on the upper branch of Figure 5. The semi-analytical temperature profile has an axisymmetric temperature peak, of 1·89 located at the centre of the reactor. The numerical solution has a temperature peak of 1·94 at $(x, y) = (0, -0{\cdot}1)$. The difference between the maximum temperatures is only 2%. The numerical temperature peak is compressed slightly in the y-direction as less heat is deposited near the waveguide walls. Moreover, the peak is displaced towards the reservoir at $y = -1$, due to the concentration of reactant being higher there. The concentration contours show a trough in the centre of the reactor, which is due to the reaction proceeding faster in the region of the maximum temperature. In the absence of any reaction ($\delta = 0$) the concentration is 0·5 at the reactor's centre. The semi-analytical and numerical concentrations for this example are 0·412 and 0·414, respectively. The electric-field amplitude shows decay of about 6% through the reactor, with the difference between the semi-analytical and numerical predictions less than 1%.

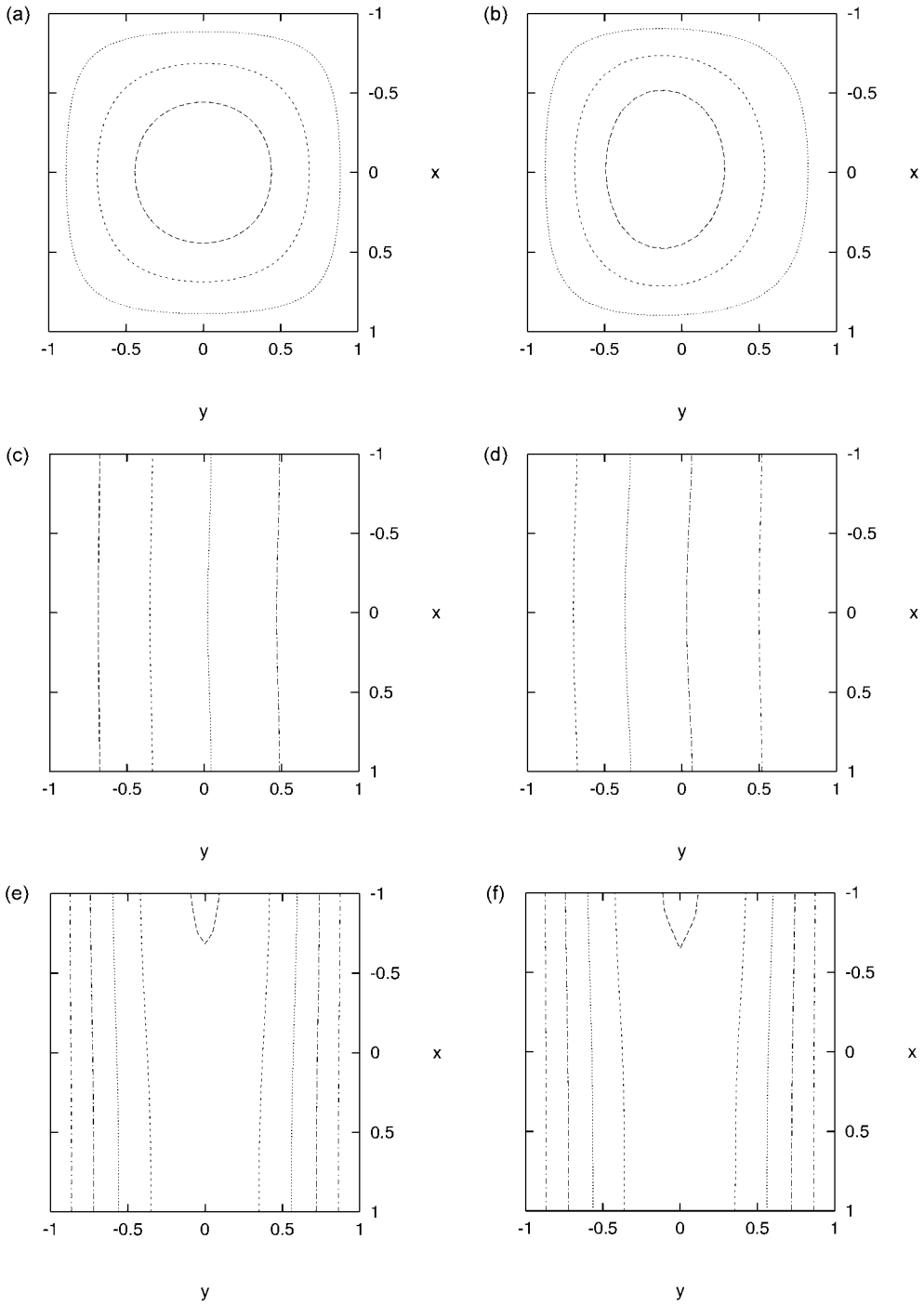

Figure 6. Steady-state temperature, concentration and electric-field amplitude contour plots for the two-dimensional reactor. Shown is the semi-analytical (a, c, e) and numerical (b, d, f) solutions. The parameters are $T_a = 0{\cdot}2$ and $\beta = 40$.

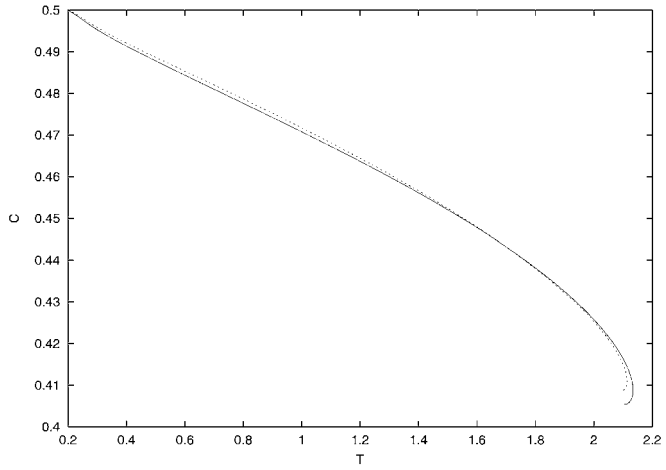

Figure 7. The evolution in the concentration versus temperature phase-plane, for the two-dimensional reactor. Shown is the semi-analytical (solid line) and numerical (dashed line) solutions. The parameters are $T_a = 0{\cdot}2$ and $\beta = 40$.

Figure 7 shows the evolution of the solution in the concentration versus temperature phase-plane. The parameters for Figure 7 are the same as for Figure 6, hence a steady-state solution results. The dominant eigenvalues from the local stability analysis are $\lambda_e = -2{\cdot}63 \pm \mathrm{i}1{\cdot}26$, which implies a stable focus. This is confirmed by the figure which shows oscillatory convergence to the steady-state solution and an excellent comparison between the semi-analytical and numerical solutions.

5. Conclusion

This paper shows the usefulness and accuracy of semi-analytical solutions for microwave reactors, illustrated by the analysis of both a one and two-dimensional microwave reactor. Comparison with numerical solutions shows the semi-analytical model to be extremely accurate, both for the steady-state solutions and for temporal evolution, such as when a limit-cycle occurs. As the semi-analytical model consists of ordinary differential equations, it can be easily analysed using the established techniques of combustion theory, such as the local stability analysis. This analysis also allows any parameter regions in which Hopf bifurcations occur to be identified.

It was found that Hopf bifurcations (and the subsequent limit-cycles) occurred for the one-dimensional reactor, but not the two-dimensional one. Future research will investigate the reason for this. The two-dimensional reactor considered here has fixed temperature and concentration conditions at the reservoir boundaries, while the one-dimensional reactor represents a system with small (but finite) Biot and Sherwood-numbers at the reservoir boundaries. So the two-dimensional reactor could be generalised to see if limit-cycles occur for finite Biot and Sherwood-numbers. Another point to investigate is the choice of temperature dependency for the thermal absorptivity. It was chosen here to be the same Arrhenius law as that governing the reaction rate. Other choices could be tried for the thermal absorptivity to determine any effect on the occurrence of limit-cycles.

Other generalisations in the microwave reactor model could involve the inclusion of more complex chemistry. Equations for the concentration of all the reactants and products could be included in the model, together with the modelling of two (or many) step reactions.

Appendix A, Integrals for the semi-analytical solutions

Below are the integrals (A1) which form the semi-analytical model for the one-dimensional reactor

$$
\begin{aligned}
I_a = {} & \frac{3g_{41}C_0a_1\pi^4\left(\mathrm{e}^{4u}-1\right)\mathrm{e}^{-2u}}{16u\left(u^2+\pi^2\right)\left(4u^2+\pi^2\right)} + \frac{12\pi^3 g_{31}C_0a_1\left(1+\mathrm{e}^{4u}\right)\mathrm{e}^{-2u}}{\left(16u^2+9\pi^2\right)\left(16u^2+\pi^2\right)} \\
& + \frac{g_{21}C_0a_1\pi^2\left(\mathrm{e}^{4u}-1\right)\mathrm{e}^{-2u}}{4u\left(4u^2+\pi^2\right)} + \frac{3\pi^4 g_{41}C_0b_1\sin(2v)}{32v^5-40v^3\pi^2+8v\pi^4} \\
& + \frac{24\cos(2v)\pi^3 g_{31}C_0b_1}{9\pi^4-160v^2\pi^2+256v^4} - \frac{\pi^2 g_{21}C_0b_1\sin(2v)}{8v^3-2v\pi^2} \\
& - \frac{4\cos(2v)\pi g_{11}C_0b_1}{-\pi^2+16v^2} + \frac{g_{21}C_1b_1\pi^2\sin(v)\cos(v)\left(2v^2+\pi^2\right)}{2v\left(4v^4-5v^2\pi^2+\pi^4\right)} \\
& + \frac{\cos(2v)b_1C_1g_{11}\pi(12\pi^2+64v^2)}{9\pi^4-160v^2\pi^2+256v^4} + \frac{2\pi g_{11}C_0a_1\left(1+\mathrm{e}^{4u}\right)\mathrm{e}^{-2u}}{16u^2+\pi^2} \\
& - \frac{3g_{41}C_1a_1\pi^4\left(2u^2-3\pi^2\right)\left(\mathrm{e}^{4u}-1\right)\mathrm{e}^{-2u}}{8u\left(4u^2+9\pi^2\right)\left(u^2+\pi^2\right)\left(4u^2+\pi^2\right)} \\
& - \frac{12\pi^3 g_{31}C_1a_1\left(16u^2-15\pi^2\right)\left(1+\mathrm{e}^{4u}\right)\mathrm{e}^{-2u}}{\left(16u^2+25\pi^2\right)\left(16u^2+9\pi^2\right)\left(16u^2+\pi^2\right)} \\
& - \frac{g_{21}C_1a_1\pi^2\left(2u^2-\pi^2\right)\left(\mathrm{e}^{4u}-1\right)\mathrm{e}^{-2u}}{8u\left(u^2+\pi^2\right)\left(4u^2+\pi^2\right)} \\
& - \frac{2\pi g_{11}C_1a_1\left(16u^2-3\pi^2\right)\left(1+\mathrm{e}^{4u}\right)\mathrm{e}^{-2u}}{\left(16u^2+9\pi^2\right)\left(16u^2+\pi^2\right)} \\
& + \frac{3g_{41}C_1b_1\pi^4\sin(v)\cos(v)\left(3\pi^2+2v^2\right)}{2v\left(56\pi^2v^4-49\pi^4v^2+9\pi^6-16v^6\right)} \\
& + \frac{\cos(2v)b_1C_1g_{31}\pi^3(360\pi^2+384v^2)}{225\pi^6-4144\pi^4v^2+8960\pi^2v^4-4096v^6},
\end{aligned}
\tag{A1}
$$

$$
I_b = g_{12} + \frac{3}{4}g_{32} + \frac{8}{3\pi}g_{22} + \frac{32}{15\pi}g_{42},
$$

$$
I_{c1i} = 2g_{1i} + g_{3i} + \frac{4}{\pi}g_{2i} + \frac{8}{3\pi}g_{4i}, \quad I_{c2i} = \frac{1}{2}g_{3i} + \frac{4}{3\pi}g_{2i} + \frac{8}{5\pi}g_{4i},
$$

$$
I_{c3i} = g_{1i} + \frac{1}{2}2g_{3i} + \frac{152}{105\pi}g_{4i} + \frac{28}{15\pi}g_{2i},
$$

and the integrals (A2) for the two-dimensional microwave reactor

$$
\begin{aligned}
I_a = {} & \frac{15g_{41}C_1b_1\pi^4\sin(v)\cos(v)\left(3\pi^2+2v^2\right)}{16v\left(56\pi^2v^4-49\pi^4v^2+9\pi^6-16v^6\right)}+\frac{15g_{41}C_0a_1\pi^4\left(\mathrm{e}^{4u}-1\right)\mathrm{e}^{-2u}}{128u\left(u^2+\pi^2\right)\left(4u^2+\pi^2\right)}\\
& -\frac{15g_{41}C_1a_1\pi^4\left(-3\pi^2+2u^2\right)\left(\mathrm{e}^{4u}-1\right)\mathrm{e}^{-2u}}{64u\left(4u^2+9\pi^2\right)\left(u^2+\pi^2\right)\left(4u^2+\pi^2\right)}+\frac{15\pi^4g_{41}C_0b_1\sin(2v)}{256v^5-320v^3\pi^2+64v\pi^4}\\
& +\frac{\pi^3g_{41}a_1\left(\mathrm{e}^{4u}-1\right)\mathrm{e}^{-2u}}{5u\left(u^2+\pi^2\right)\left(4u^2+\pi^2\right)}+\frac{2\pi^3g_{41}b_1\sin(2v)}{20v^5-25v^3\pi^2+5v\pi^4}\\
& -\frac{128\pi^2g_{31}a_1C_1\left(16u^2-15\pi^2\right)\left(1+\mathrm{e}^{4u}\right)\mathrm{e}^{-2u}}{5\left(16u^2+25\pi^2\right)\left(16u^2+9\pi^2\right)\left(16u^2+\pi^2\right)}\\
& +\frac{\cos(2v)C_1b_1g_{31}\pi^2(3840\pi^2+4096v^2)}{1125\pi^6-20720\pi^4v^2+44800\pi^2v^4-20480v^6}\\
& +\frac{128\pi^2g_{31}a_1C_0\left(1+\mathrm{e}^{4u}\right)\mathrm{e}^{-2u}}{5\left(16u^2+9\pi^2\right)\left(16u^2+\pi^2\right)}-\frac{2\pi g_{21}b_1\sin(2v)}{12v^3-3v\pi^2}\\
& +\frac{256\pi^2g_{31}b_1C_0\cos(2v)}{45\pi^4-800v^2\pi^2+1280v^4}-\frac{3a_1g_{21}C_1\pi^2\left(2u^2-\pi^2\right)\left(\mathrm{e}^{4u}-1\right)\mathrm{e}^{-2u}}{32u\left(u^2+\pi^2\right)\left(4u^2+\pi^2\right)}\\
& +\frac{3g_{21}C_0a_1\pi^2\left(\mathrm{e}^{4u}-1\right)\mathrm{e}^{-2u}}{16u\left(4u^2+\pi^2\right)}+\frac{3g_{21}b_1C_1\pi^2\sin(v)\cos(v)\left(2v^2+\pi^2\right)}{8v\left(4v^4-5v^2\pi^2+\pi^4\right)}\\
& +\frac{9\pi^3g_{31}b_1\cos(2v)}{9\pi^4-160v^2\pi^2+256v^4}+\frac{9\pi^3g_{31}a_1\left(1+\mathrm{e}^{4u}\right)\mathrm{e}^{-2u}}{2\left(16u^2+9\pi^2\right)\left(16u^2+\pi^2\right)}\\
& +\frac{16g_{11}a_1C_0\left(1+\mathrm{e}^{4u}\right)\mathrm{e}^{-2u}}{3(16u^2+\pi^2)}+\frac{\pi g_{21}a_1\left(\mathrm{e}^{4u}-1\right)\mathrm{e}^{-2u}}{3u\left(4u^2+\pi^2\right)}-\frac{3\pi^2g_{21}C_0b_1\sin(2v)}{32v^3-8v\pi^2}\\
& -\frac{16C_1a_1g_{11}\left(16u^2-3\pi^2\right)\left(1+\mathrm{e}^{4u}\right)\mathrm{e}^{-2u}}{3\left(16u^2+9\pi^2\right)\left(16u^2+\pi^2\right)}+\frac{\cos(2v)g_{11}b_1C_1(96\pi^2+512v^2)}{27\pi^4-480v^2\pi^2+768v^4}\\
& -\frac{32g_{11}b_1C_0\cos(2v)}{48v^2-3\pi^2}+\frac{g_{11}\pi a_1\left(1+\mathrm{e}^{4u}\right)\mathrm{e}^{-2u}}{16u^2+\pi^2}-\frac{2g_{11}\pi b_1\cos(2v)}{16v^2-\pi^2},
\end{aligned}
\tag{A2}
$$

$$
I_b = g_{12}+\frac{9}{16}g_{32}+\frac{64}{9\pi^2}g_{22}+\frac{1024}{225\pi^2}g_{42},
$$

$$
I_{c1i} = \frac{8}{\pi}g_{1i}+\frac{4}{\pi}g_{2i}+\frac{8}{3\pi}g_{3i}+\frac{2}{\pi}g_{4i},\quad I_{c2i} = \frac{3}{8}g_{3i}+\frac{32}{9\pi^2}g_{2i}+\frac{256}{75\pi^2}g_{4i},
$$

$$
I_{d1i} = \frac{2}{15\pi}(10g_{2i}+9g_{4i}+10g_{3i}),
$$

$$
I_{d2i} = \frac{19}{21\pi}g_{4i}+\frac{16}{15\pi}g_{3i}+\frac{8}{3\pi}g_{1i}+\frac{7}{5\pi}g_{2i},
$$

$$
I_{e1} = 2g_{11}+\frac{1}{2}g_{31}+\frac{32}{9\pi^2}g_{41}+\frac{8}{\pi^2}g_{21},
$$

$$I_{e2} = \frac{2}{3\pi}g_{21} + \frac{3}{5\pi}g_{41} + \frac{2}{3\pi}g_{31},$$

$$I_{f1} = 2g_{11} + \frac{1}{2}g_{31} + \frac{4}{3\pi}g_{21}C_1 + \frac{4}{3\pi}g_{31}C_1 + \frac{8}{\pi}g_{11}C_0 + \frac{2}{\pi}g_{41}C_0$$
$$+\frac{6}{5\pi}g_{41}C_1 + \frac{4}{\pi}g_{21}C_0 + \frac{8}{3\pi}g_{31}C_0 + \frac{32}{9\pi^2}g_{41} + \frac{8}{\pi^2}g_{21},$$

$$I_{f2} = 4g_{12} + g_{32} + \frac{16}{\pi^2}g_{22} + \frac{64}{9\pi^2}g_{42}.$$

Both sets of integral use the common expressions

$$\begin{aligned} g_{1i} &= r_{i0} + r_{i1}T_a + r_{i2}T_a^2 + r_{i3}T_a^3, \\ g_{2i} &= r_{i1}T_0 + 2r_{i2}T_aT_0 + 3r_{i3}T_a^2T_0, \\ g_{3i} &= r_{i2}T_0^2 + 3r_{i3}T_0^2T_a,\ \ g_{4i} = r_{i3}T_0^3. \end{aligned} \tag{A3}$$

Appendix B, Numerical model

Here the numerical scheme for the governing equations of the one-dimensional microwave reactor is presented. The scheme for the two-dimensional reactor is obtained with appropriate modifications.

For the one-dimensional case, the solution is

$$\begin{aligned} &T = [T_i^n],\ \ c = [c_i^n],\ \ U = [U_i^n], \\ &T_i^n = T(-1 + (i-1)\Delta x, (n-1)\Delta t), \\ &c_i^n = c(-1 + (i-1)\Delta x, (n-1)\Delta t), \\ &U_i^n = U(-1 + (i-1)\Delta x, (n-1)\Delta t), \end{aligned} \tag{B1}$$

where $i = 1, \ldots, h \quad n = 1, \ldots, h = 1 + \frac{2}{\Delta x}$. The governing equations (13) are discretised to become

$$\begin{aligned} &T_i^{n+1} = T_i^n + s(T_{i-1}^n + T_{i+1}^n - 2T_i^n) \\ &+\Delta t\beta c_i^n Ar(T_i^n)|U_i^n|^2 + \Delta t g(T_a - T_i^n), \\ &c_i^{n+1} = c_i^n + s(c_{i-1}^n + c_{i+1}^n - 2c_i^n) \\ &-\Delta t\delta c_i^n Ar(T_i^n) + \Delta t r(1 - c_i^n), \\ &U_{i+1}^n + U_{i-1}^n - 2U_i^n + \Delta x^2 k_1^2(1 + \alpha c_i^n Ar(T_i^n))U_i^n = 0, \end{aligned} \tag{B2}$$

where $i = 1, \ldots, h, n = 1, \ldots$ and $s = \frac{\Delta t}{\Delta x^2}$. This represents the explicit FTCS method for the heat and concentration equations, which is stable for $s < 0{\cdot}5$. The accuracy of the numerical scheme is $O(\Delta x^2, \Delta t)$. The boundary conditions (14) become

$$\begin{aligned} &T_1^n = T_h^n = T_a,\ \ c_2^n = c_0^n,\ \ c_{h+1}^n = c_{h-1}^n, \\ &U_2^n - U_0^n + 2\Delta x i k_r U_1^n = 4\Delta x k_r, \\ &U_{h+1}^n - U_{h-1}^n - 2\Delta x i k_r U_h^n = 0. \end{aligned} \tag{B3}$$

The matrix form for the discretised Helmholtz equation (B2) is

$$A\mathbf{U}' = \mathbf{d}, \tag{B4}$$

where the vector $\mathbf{U}'$ represents the electric-field amplitude U. The form of (B4) is chosen so the matrix A has constant coefficients. All the nonlinear Arrhenius terms of (B2) are placed in the right-hand side $\mathbf{d}$ of the equation (B4). The matrix A is reduced to upper triangular form whilst the lower triangular matrix which performs the reduction is stored for later use. As A has constant coefficients this reduction to upper triangular form is only performed once. When the temperature and concentration at the time level $t = (n+1)\Delta t$ has been found it is used in the right-hand side of (B4), which is then solved via the iteration procedure

$$A\mathbf{U}'_{(n+1)} = \mathbf{d}_{(n)}, \quad n = 0, 1, 2, 3 \ldots , \tag{B5}$$

where each iteration step requires one matrix multiplication and a back-substitution. As the initial guess for $\mathbf{U}'$ is the solution at the old time-level and the time step Δt is small the iteration usually needs only one or two steps are needed to converge.

References

1. C. R. Strauss. A combinatorial approach to the development of environmentally benign organic chemical preparations. *Aust. J. Chem.* 52 (1999) 83–96.
2. A. Zlotorzynski. The application of microwave radiation to analytical and environmental chemistry. *Crit. Rev. Anal. Chem.* 25 (1995) 43–76.
3. B. Liu and T. R. Marchant. The microwave heating of two-dimensional slabs with small Arrhenius absorptivity. *IMA J. Appl. Math.* 62 (1999) 137–162.
4. G. A. Kriegsmann. Thermal runaway and its control in microwave heated ceramics. *Mat. Res. Soc. Symp. Proc.* 269 (1992) 257–264.
5. B. Liu and T. R. Marchant. On the occurrence of limit-cycles during feedback control of microwave heating. *J. Math. Computer Model.* (2002) to appear.
6. M. R. Booty, J. K. Bechtold and G. A. Kriegsmann. Microwave-induced combustion: a one-dimensional model. *Combust. Theory Modelling* 2 (1998) 57–80.
7. B. S. Tilley and G. A. Kriegsmann. Microwave enhanced chemical vapor infiltration: a sharp interface model. *J. Engng. Math.* 41 (2001) 33–54.
8. F. Chemat, D. C. Esveld, M. Poux and J. L. DiMartino. The role of selective heating in the microwave activation of heterogeneous catalysis reactions using a continuous microwave reactor. *J. Microwave Power and Electromagnetic Energy* 33 (1998) 88–94.
9. L. K. Forbes. Limit-cycle behaviour in a model chemical reaction: the Sal'nikov thermokinetic oscillator. *Proc. R. Soc. Lond. A* 430 (1990) 641–651.
10. A. R. Von Hippel, *Dielectric materials and applications*. Cambridge: MIT press (1954) 438 pp.
11. D. Acierno, V. Fiumara, M. Frigione, D. Napoli, I. M. Pinto and M. Ricciardi. Comparative study of microwave and thermal curing of epoxy resins. In: J. M. Catala-Civera, F. L. Penaranda-Foix, D. Sanchez-Hernandez, and E. de los Reyes (eds.): *7th Inter. Conf. on Microwave and High-Frequency Heating*. (1999) pp. 209–212.
12. G. A. Kriegsmann. Cavity effects in microwave heating of ceramics. *SIAM J. Appl. Math.* 57 (1997) 382–400.
13. J. H. Merkin, J. H., V. Petrov, S. K. Scott and K. Showalter. Wave-induced chaos in a continuously fed unstirred reactor. *J. Chem. Soc., Faraday Trans.* 92 (1996) 2911–2918.
14. J. M. Hill and M. J. Jennings. Formulation of model equations for heating by microwave radiation. *Appl. Math. Modelling* 17 (1993) 369–379.
15. M. Golubitsky and D. G. Schaeffer, *Singularities and Groups in Bifurcation Theory*. New York: Springer-Verlag (1985) 463 pp.
16. T. R. Marchant. Cubic autocatalytic reaction-diffusion equations: semi-analytical solutions. *Proc. R. Soc. London A* 458 (2002) 873–888.